JOURNAL OF THERMOPHYSICS AND HEAT TRANSFER
Vol. 19, No. 3, July–September 2005

Reverse Monte Carlo Simulations of Light Pulse Propagation Within Three-Dimensional Media

Xiaodong Lu* and Pei-feng Hsu†
Florida Institute of Technology, Melbourne, Florida 32901-6988

An ultrashort light pulse inside an absorbing and anisotropically scattering three-dimensional nonhomogeneous medium is considered. The purpose is two fold: to develop an accurate and easily parallelized numerical model to understand the physics of the transport process and to provide a tool with which a direct comparison with measured temporal signals can be made. The ultrashort light pulse propagation is modeled by the reverse Monte Carlo method. The detailed algorithm treating the source integration over a path length that contains nonuniform radiative properties and finite-size collimated source is given. Validation and numerical simulations are presented. It is found that there is a direct correlation between the travel time of ballistic photons in the temporal reflectance signals and the interface location under certain conditions. It is also found that the inversion parameters proposed by earlier research, such as the long-time logarithm slope and pulse-broadening effect, are inadequate for use in the inverse analysis because these parameters do not provide the specificity needed for such use. More study is needed to identify effective inversion parameters.

Nomenclature

a	=	absorption coefficient, m^{-1}
c	=	propagation speed of radiation transport in the medium, m/s
d	=	pulse spatial width
g	=	pulse spatial and/or temporal shape function
I	=	radiation intensity, W/m^2sr
I_0	=	radiation intensity at boundary $z = 0$
L_0	=	total slab thickness, m
N	=	number of samplings or energy bundles
r	=	radial coordinate, m
$\hat{r}$	=	position vector of a location (x, y, z) in space
s	=	geometric path length, m
$\hat{s}$	=	unit vector along a given direction
t	=	time, s
x, y, z	=	rectangular coordinates, m
κ	=	extinction coefficient, $\kappa = a + \sigma$, m^{-1}
μ_z	=	direction cosine in z-direction
σ	=	scattering coefficient, m^{-1}
τ_i	=	optical thickness of the ith layer, $\kappa_i L_i$
Φ	=	scattering phase function
Ω	=	solid angle, sr
ω	=	scattering albedo

Subscripts

abs	=	absorption
d	=	direct attenuation component; detector location
ext	=	extinction
k	=	path length index
L	=	lower limit of path length segment l_k integration
n	=	index of N samplings
o	=	collimated pulse direction
p	=	pulse
s	=	multiply scattered or diffuse component
seg	=	path length segment, i.e., l_k
U	=	upper limit of path length segment l_k integration
w	=	wall or surface position

Superscripts

$'$	=	dummy variables
$''$	=	dummy variables
$\hat{}$	=	vector
$+$	=	upper bound of integration limit
$-$	=	lower bound of integration limit
$\perp$	=	direction normal to z axis
r	=	travel time of photons from incident point to and back from the interface

I. Introduction

THE transient radiative process has diverse applications in astrophysics, thermal systems, biomedical imaging, remote sensing, etc. Various analytical models have been developed over the years, from the early diffusion approximation and its variants to the discrete-ordinates method and the recently developed, rigorous integral equation models. Kumar et al.[1] described several commonly used deterministic models. However, all the deterministic models have various computational, model fidelity, and scaling issues. For example, although the diffusion approximations is computationally efficient, it failed to predict the photon behavior in the initial transient, including the propagation speed. The commonly used discrete-ordinates and finite-volume methods are relatively efficient in computational time. Nevertheless, the large memory requirement and the communication overhead make these methods difficult when an effective parallel scheme is deployed for complex or large-scale problems. The problem also appears in other differential treatments of the radiative transport equation. The integral formulation has very good parallel efficiency and accuracy but is not easy to use in the case of reflective boundary.[2]

On the other hand, the stochastic approach of the Monte Carlo (MC) method has long been considered a benchmark tool that is amicable to various model fidelity requirements, although not computationally efficient. The key idea of stochastic methods is to treat the solution as the theoretically expected value of a random variable that is defined in the probability measure space. The expected value

Presented as Paper 2004-2680 at the 37th Thermophysics Conference, Portland, OR, 28 June–1 July 2004; received 10 July 2004; revision received 11 October 2004; accepted for publication 12 October 2004.

*Doctoral Candidate, Mechanical and Aerospace Engineering Department, 150 West University Boulevard. Student Member AIAA.

†Professor of Mechanical Engineering, Mechanical and Aerospace Engineering Department, 150 West University Boulevard; phsu@fit.edu. Associate Fellow AIAA.

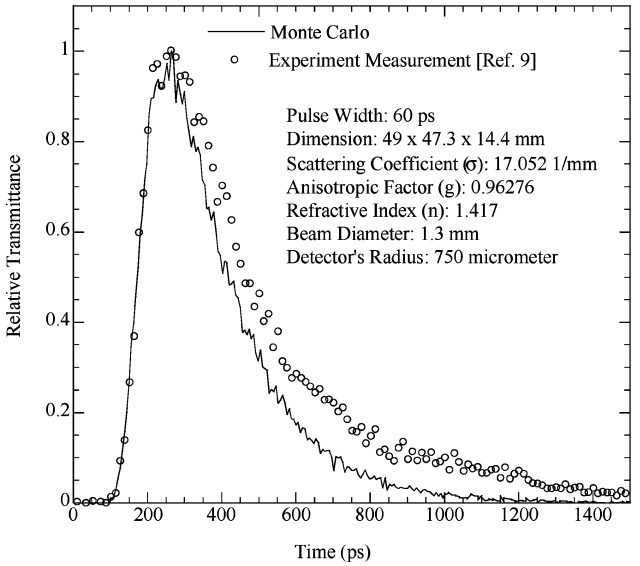

Fig. 1 Comparison of experimental measurement of temporal transmittance of light pulse through a rectangular medium and Monte Carlo simulated result.

is then approximated by sample means. One main advantage of MC integrations is the computational cost is insensitive to the dimensionality of the integral, but dependent on the sample size.[3] That is why MC is very suitable for solving very complex problems. The computational cost is proportional to the number of samplings and has little to do with the dimensionality of the geometry.

The MC simulation of light pulse propagation is very time-consuming, even in parallel systems.[4] The alternative is to use the reverse Monte Carlo (RMC) method, as demonstrated in our previous work.[5–7] This is an expansion of the prior one-dimensional geometry study to three-dimensional geometry and to providing simulation tools that are efficient, accurate, and scalable to parallel computing systems for geometrically complex problems. This tool will allow direct comparison with experimental data and perform inverse analysis. The latter is best carried out in a parallel system, for example, a Beowulf cluster.[8]

Figure 1 is a comparison of MC simulation of light pulse transmitted signals with measurement[4,9] in a homogeneous, highly scattering sample. The numerical and experimental data appear to follow the same temporal characteristics as reported by many. However, there are two issues with the comparison and in fact they are the same issues that exist in data reported in the literature: the simulation and actual signal have to be normalized with their respective peak values, and even more problematic is the shifting of the $t = 0$ point so that a better agreement can be obtained. With the given sample thickness of 14.4 mm, the ballistic photon is predicted to emerge 74 ps after entering the front surface. The MC simulation shows that the first signal appears at about 90 ps under the given conditions. The experimental measurements are shifted in time to match the peak of MC simulation. The main discrepancy between MC simulation and experiment is the disparity in the temporal width of the transmittance tail. The MC simulation exhibits oscillations near the peak and much larger oscillations versus absolute signal magnitude ratio at long time. More work is obviously needed to improve the experimental accuracy and resolution as well as the numerical simulation.

Conventional (or forward) Monte Carlo is efficient if the radiation source is confined to a small volume and/or a solid angle, whereas reverse Monte Carlo is efficient if radiative flux or incident radiation at a small surface and/or over a small solid angle is needed. Both methods become inefficient if radiation is emitted from a small source and the radiative flux onto a small detector is of interest, as shown in Ref. 10. However, in transient processes the RMC method is still preferred over the MC method, because in some cases only a portion of the temporal radiative signal is needed and RMC can provide a solution at a given time or over a time interval in the so-called "time-gating" measurement.[11] On the other hand, the MC method will require simulation from the very beginning to the time of interest.[1] The RMC method has advantages in applications where only information at certain locations and finite solid angles and/or time is needed. Examples are remote sensing, optical imaging, and many other inverse analysis applications.

Unlike our previous work on one-dimensional geometry,[5–7] the current problem has a pulsed, finite-size beam moving in space, and the chance of backtracking bundles to encounter the source is even smaller. The situation requires a significantly larger number of bundles (and computational time) for multidimensional simulation. A possible solution is to send the bundles in the directions according to a modified cumulative distribution function.[12] The idea is to send the backtracking bundles in the directions that have a greater chance of encountering the moving pulse source. In this study, we will establish basis results without resorting to the biased directions. A future study will consider such strategy and compare the improvement in computational time and accuracy.

There are several good discussions on using the reverse or backward Monte Carlo method, for example, Nelson,[13] Walter and Buckius,[14] and recently Modest.[10] However, these are only for steady state problems. Furthermore, there are only a very limited numbers of RMC simulations of the pulse propagation inside the scattering media. To the best of the authors' knowledge, a detailed discussion of the algorithm is not available in the literature. A general transient algorithm to deal with multidimensional, nonhomogeneous media is especially needed and presented here.

This paper presents an expansion on the one-dimensional models previously developed by the authors.[5–7] Although no new concept is needed to extend to multidimensional geometry, the new algorithm needs to consider the finite-sized light pulse and the nonuniform radiative properties along the energy bundle's backtracking path and along the light pulse's path. These are not trivial and detailed description is presented. It is therefore important to present a validated RMC algorithm for simulating the light pulse movement in realistic geometry and property conditions.

II. Transient Radiative Transfer Equation

The problem under consideration is a collimated, ultrashort pulsed irradiation on the top surface of a rectangular medium. The light pulse's temporal width is on the order of pico- or femtoseconds. The geometry is shown in Fig. 2.

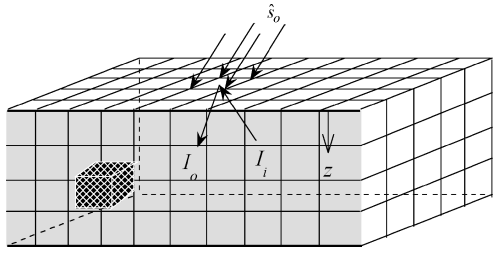

a) Rectangular medium and coordinate system

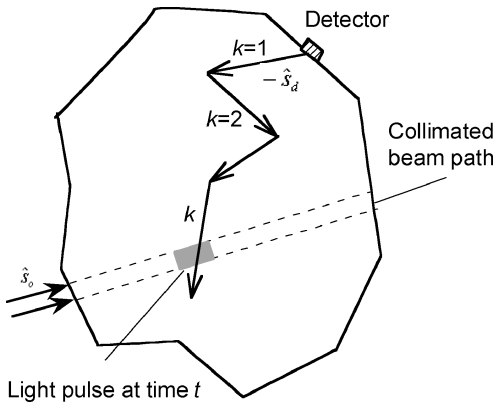

b) Backtracking bundle's movement

Fig. 2 Geometry of the collimated irradiation.

In Fig. 2a, $I(\hat{s}_0, t)$ is the collimated irradiation intensity in direction $\hat{s}_0$. I_0 is the intensity leaving the wall toward the medium and I_i the intensity coming from the medium toward the wall. The light pulse irradiates one surface element and the shaded volume element represents the smallest medium volume size that has radiative properties different from those of the surrounding medium. The detector of radiation signals, radiative flux over a finite solid angle, can be placed anywhere in the medium. Most common applications will have one or more detectors placed at the enclosure surface.

The medium is absorbing, scattering, and nonemitting and assumed to be cold and gray. The enclosure surface is considered to be a Fresnel reflective surface. The radiative transfer equation (RTE) to describe the light intensity in a given direction $\hat{s}$ is given as[15]

$$\frac{\partial I(\hat{r}, \hat{s}, t)}{c\partial t} + \frac{\partial I(\hat{r}, \hat{s}, t)}{\partial s} = -\kappa(\hat{r}) I(\hat{r}, \hat{s}, t) + \frac{\sigma(\hat{r})}{4\pi} \int_{\Omega'=4\pi} I(\hat{r}, \hat{s}', t)\Phi(\hat{r}, \hat{s}', \hat{s})\, \mathrm{d}\Omega' \tag{1}$$

where κ and σ are the position-dependent extinction coefficient and the scattering coefficient, respectively, and $\kappa = a + \sigma$; c is the speed of light in the medium, $\hat{s}$ the light propagation direction, and $\Phi(\hat{r}, \hat{s}', \hat{s})$ the scattering phase function. It is assumed that the model, that is, Eq. (1), is suitable to describe the light pulse propagation in the participating media.[16] The temporal radiative signals, for example, transmittance and reflectance, are usually of interest. In inverse analysis and remote sensing applications, the temporal information is used to determine the material composition, existence of inhomogeneity (and if it exists, its location), and so on. Several deterministic numerical schemes have been developed to solve Eq. (1) (Ref. 1). However, these are all subject to various modeling or numerical issues. In the next section, a new method of solving the transient radiative transport equation based on the reciprocity principal of optics[17] and Monte Carlo stochastics is described.

III. Reverse Monte Carlo Method

It is convenient to use a concept similar to Olfe's[18] modified differential approximation by splitting the intensity into two components: one contributed by incident radiation and the other by medium emission and scattering. The former can be solved exactly with the boundary condition containing singular emission source and the latter by various numerical schemes:

$$I(\hat{r}, \hat{s}, t) = I_d(\hat{r}, \hat{s}, t) + I_s(\hat{r}, \hat{s}, t) \tag{2}$$

where $I_d(\hat{r}, \hat{s}, t)$ is the component contributed directly by the collimated irradiation at position $\hat{r}$ in direction $\hat{s}$ and $I_s(\hat{r}, \hat{s}, t)$ is the multiply scattered component. From this treatment it is easy to show that I_d solution can be obtained through the direct attenuation,

$$I_d(\hat{r}, \hat{s}, t) = g_0(\hat{r}, t)\delta(\hat{s} - \hat{s}_0) \exp\left[-\int \kappa(\hat{r}')\, \mathrm{d}s' \right] \tag{3}$$

$g_0(\hat{r}, t)$ is the pulse shape function at the surface, and δ is the Dirac delta distribution. The "source term" in the RTE is resulted from the scattering of the collimated beam and is given as

$$S(\hat{r}, \hat{s}, t) = g_0(\hat{r}, t)\sigma(\hat{r}) \exp\left[-\int \kappa(\hat{r}')\, \mathrm{d}s' \right] \frac{\Phi(\hat{r}, \hat{s}_0, \hat{s})}{4\pi} \tag{4}$$

The reverse Monte Carlo algorithm of backtracking N energy (or photon) bundles from the point of interest, for example, the detector (see Fig. 2b), to simulate the diffuse component of the intensity at $\hat{r}_d$ (say, a detector position) in the $\hat{s}_d$ direction is based on the principle of reciprocity and time-reflection symmetry of Φ,[5,16,19]

$$I_n(\hat{r}_d, \hat{s}_d, t) = \int_0^l S(\hat{r}', -\hat{s}', t') \exp\left[-\int_0^{l'} a(\hat{r}'')\, \mathrm{d}l'' \right] \mathrm{d}l' \tag{5}$$

The $\hat{s}'$ is the direction of the backtracking bundle's movement inside the medium, starting with $\hat{s}' = -\hat{s}_d$ (Fig. 2b). The exponential term in the above equation is based on the "absorption suppression" described by Walter and Buckius.[14]

IV. Reverse Monte Carlo Method in Three-Dimensional Geometry

Consider a light pulse with a "top-hat" temporal shape, a rectangular spatial cross section, and $\hat{s}_0$ pointing to the z-direction,

$$S(\hat{r}, \hat{s}, t) = \lfloor H(ct - z) - H(ct - ct_p - z) \rfloor [H(x_2 - x) - H(x_1 - x)] [H(y_2 - y) - H(y_1 - y)] \sigma(\hat{r}) \exp\left[-\int_0^{l_c} \kappa(\hat{r}')\, \mathrm{d}l_c' \right] \frac{\Phi(\hat{r}, \hat{s}_0, \hat{s})}{4\pi} \tag{6}$$

where H is the Heaviside step function, $x_2 - x_1 = y_2 - y_1 = d$, d the width of the pulse cross section, and l_c the distance that the collimated pulse travels from the boundary $\hat{r}_w$ to the current location $\hat{r}(x, y, z)$. Equation (6) uses a more specific form of the pulse shape function inside the medium in Eq. (4).

It should be pointed out that a pulse of circular cross section with spatial Gaussian profile could be implemented in the model. However, it is expected that the pulse temporal and spatial shapes have much less influence on the radiative signals than the pulse width.[20] The use of a top-hat pulse shape and rectangular cross section will have a minimum impact on the simulated signals but simplify the calculation. In simulations, d will be the effective diameter of the laser beam. For the problem under consideration we also neglect the reflection of I_d at the internal boundary surfaces because the media for such applications typically have very high optical thickness and I_d magnitude rapidly decreases to a very small value after one pass inside the media. Although the internal boundary reflection of I_d can be incorporated into the MC simulation, the extra modeling complexities do not warrant the insignificant improvement in the resulting solution.

In the three-dimensional geometry, Eq. (5) becomes

$$\begin{aligned} I_n(r_d, \hat{s}_d, t) &= \int_0^l S(r(l'), -\hat{s}', t') \exp\left[-\int_0^{l'} a(r(l''))\, \mathrm{d}l'' \right] \mathrm{d}l' \\ &= \frac{1}{4\pi} \int_0^l [H(ct - z) - H(ct - ct_p - z)] [H(x_2 - x) - H(x_1 - x)] [H(y_2 - y) - H(y_1 - y)] \\ &\quad \sigma(r(l'))\Phi(r(l'), \hat{s}_0, -\hat{s}') \\ &\quad \times \exp\left[-\int_0^{l_c'} \kappa(r(l_c''))\, \mathrm{d}l_c'' - \int_0^{l'} a(r(l''))\, \mathrm{d}l'' \right] \mathrm{d}l' \\ &= \frac{1}{4\pi} \sum_k \int_{l_k^-}^{l_k^+} \sigma(r(l'))\Phi(r(l'), \hat{s}_0, -\hat{s}') \\ &\quad \times \exp\left[-\int_0^{l_c'} \kappa(r(l_c'))\, \mathrm{d}l_c' - \int_0^{l'} a(r(l''))\, \mathrm{d}l'' \right] \mathrm{d}l' \end{aligned} \tag{7}$$

where l_k is the bundle's kth straight backtracking segment within the l, which is the travel distance of the backtracking bundle when it encounters the backward-moving collimated pulse. The nonhomogeneous property in the path integration is handled by separating each l_k segment into sections which are the travel path lengths in each individual homogeneous rectangular volume cell (Fig. 3). Equation (7) can be written as

$$I_n(\hat{r}_d, \hat{s}_d, t) = \frac{1}{4\pi} \sum_k \sum_i \sigma_{k,i}\Phi(\hat{r}, \hat{s}_0, -\hat{s}_k') \int_{l_{k,i}^-}^{l_{k,i}^+} \times \exp\left(-\sum_{j=1}^{m_{k,i}} \kappa_j \Delta z_j - \sum_{h=1}^{n_{k,i}} a_h \Delta l_h \right) \mathrm{d}l_i' \tag{8}$$

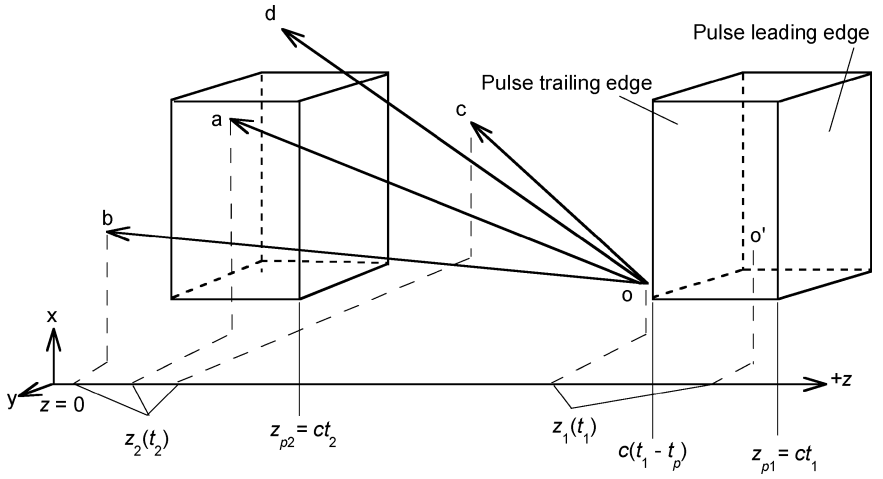

Fig. 3 Backtracking bundle path length and pulse movement in the medium.

where the subscript i refers to the ith cell in the kth path segment, $m_{k,i}$ is the number of volume cells the collimated beam has crossed before reaching the location in the ith cell at the time when it encounters the backtracking bundle, and $n_{k,i}$ is the number of cells the backtracking bundle has crossed before it reaches the same location. It is obvious that $\hat{s}_k = -\hat{s}_s$ when $k = 1$. The indices $m_{k,i}$ and $n_{k,i}$ both point to the same cell. The first term inside the exponential function in Eq. (8) represents the attenuation of the collimated beam intensity and the second term is the absorption suppression of the backtracking bundle's intensity.

The detailed RMC algorithm is discussed in Ref. 5 for one-dimensional geometry and in Ref. 6 for nonhomogeneous media. Below we will discuss the additional considerations for three-dimensional, nonhomogeneous media. The major issue in the homogeneous RMC algorithm is to determine whether and where the backtracking bundle will encounter the moving source, that is, the collimated pulse, and the locations of these encounters.[5] In one-dimensional layered nonhomogeneous media, the treatment of the source integration is more involved than that in the homogeneous case because of the variation of radiative properties (including κ, a, and Φ) along the bundle path length and the pulse moving path.[6] In three-dimensional problems, though the relations for source integration remain almost unchanged, implementation of Eq. (7) is even more complex due to the finite temporal width and finite spatial size of the light pulse and the variation of radiative properties among the cells along the integration path l_k. The crossover or overlap path length between the backtracking bundle and the moving source is the integration path needed in Eq. (8). Because the pulse and the bundle are both moving in space, the crossover path length end points have to be determined along with the integration limits, that is, $l^+_{k,i}$ and $l^-_{k,i}$. There are four possible scenarios and three of them are the same as in Ref. 5. These cases are depicted in Fig. 3 and discussed in detail below.

In Fig. 3, the current bundle position is at location o with coordinate (x_1, y_1, z_1) at time t_1 and $t_1 > t_2$. At t_1, the light pulse's leading edge is at z_{p1} $(=c\cdot t_1)$. The z-direction pulse length is ct_p and the size in x and y direction is d. Four path lengths, $\overline{oa}$, $\overline{ob}$, $\overline{oc}$, and $\overline{od}$, are all equal to the pulse travel distance $(z_{p1} - z_{p2})$. Except $\overline{ob}$ and $\overline{oc}$, two other path lengths pass through the pulse at certain times during the bundle's backtracking from t_1 to t_2. Backtracking path $\overline{oa}$ has end point a inside the pulse at t_2. $\overline{ob}$ path ends at point b behind the pulse trailing edge or plane but does not pass through the pulse at any time between t_1 and t_2. In fact, in this case the energy bundle is falling behind the pulse propagation. $\overline{od}$ has a portion that passes though the pulse. The end point d has z coordinate within the pulse leading and trailing edges' z coordinates but does not reside inside the pulse like point a.

Another possible scenario is that the starting point of backtracking bundle is o', that is, inside the pulse at time t_1. The consideration is no different from cases discussed earlier. Of course, the lower integration limit of Eq. (7) starts with point o'. The details of determining the lower and upper integration limits were given in Lu and Hsu.[5] For brevity, the discussions are not repeated here.

Let $I_{\text{seg}}(l_k)$ be the kth straight path integration; then

$$I_n(r_d, \hat{s}_d, t) = \sum_k I_{\text{seg}}(l_k) \tag{9}$$

There are two different situations to consider for the segment integrations depending on whether the backtracking direction is perpendicular to the z axis:

1) $\mu_{z_k} \neq 0$, the backtracking direction is not perpendicular to the z axis:

$$I_{\text{seg}}(l_k) = \frac{1}{4\pi} \sum_i \sigma_{m_{k,i}} \Phi(\hat{r}, \hat{s}_0, -\hat{s}'_k) \exp\left(- \sum_j^{m_{k,i}-1} \kappa_j \Delta z_j \right.$$

$$\left. + \kappa_{m_{k,i}} z_{k,i_U} - \sum_h^{n_{k,i}-1} a_h \Delta l_h + a_{n_{k,i}} \frac{z_{k,i_L}}{\mu_{z_k}} \right)$$

$$\times \int_{l^-_{k,i}}^{l^+_{k,i}} \exp\left[-\frac{\kappa_{m_{k,i}} z}{\mu_{z_k}} \left(\mu_{z_k} + 1 - \omega_{m_{k,i}} \right) \right] \mathrm{d}\frac{z}{\mu_{z_k}} \tag{10}$$

a) $\mu_{z_k} + 1 - \omega_{m_{k,i}} \neq 0$

$$I_{\text{seg}}(l_k) = \frac{1}{4\pi} \sum_i \frac{\omega_{m_{k,i}} \Phi(\hat{r}, \hat{s}_0, -\hat{s}'_k)}{\mu_{z_k} + 1 - \omega_{m_{k,i}}}$$

$$\times \exp\left(- \sum_j^{m_{k,i}-1} \kappa_j \Delta z_j + \kappa_{m_{k,i}} z_{k,i_U} - \sum_h^{n_{k,i}-1} a_h \Delta l_h + a_{n_{k,i}} \frac{z_{k,i_L}}{\mu_{z_k}} \right)$$

$$\times \exp\left(-\kappa_{m_{k,i}} z - a_{m_{k,i}} \frac{z}{\mu_{z_k}} \right) \Bigg|_{z_{k,i_U}}^{z_{k,i_L}} \tag{11}$$

Define the extinction distance as

$$l_{\text{ext}}(z) = \sum_j \kappa_j \Delta z_j + \kappa_{m_{k,i}} \left(z - z_{k,i_U} \right)$$

and the absorption distance as

$$l_{\text{abs}}(z) = \sum_h a_h \Delta l_h + a_{n_{k,i}} \left(\frac{z - z_{k,i_L}}{\mu_{z_k}} \right)$$

The total intensity can be expressed as

$$I_n(r_d,\hat{s}_d,t)=\frac{1}{4\pi}\sum_k\sum_i\frac{\omega_{m_{k,i}}\Phi(\hat{r},\hat{s}_0,-\hat{s}'_k)}{\mu_{z_k}+1-\omega_{m_{k,i}}}\times\left\{\exp\left[-l_{\text{ext}}\left(z_{k,i_L}\right)-l_{\text{abs}}\left(z_{k,i_L}\right)\right]-\exp\left[-l_{\text{ext}}\left(z_{k,i_U}\right)-l_{\text{abs}}\left(z_{k,i_U}\right)\right]\right\} \tag{12}$$

b) $\mu_{z_k}+1-\omega_{m_{k,i}}=0$. Let $I_{\text{seg}}(l_{k,i})$ be the ith cell in the kth straight path integration:

$$I_{\text{seg}}(l_{k,i})=\frac{1}{4\pi}\sigma_{m_{k,i}}\Phi(\hat{r},\hat{s}_0,-\hat{s}'_k)\cdot\exp\left(-\sum_j^{m_{k,i}-1}k_j\Delta z_j+k_{m_{k,i}}z_{k,i_U}-\sum_h^{n_{k,i}-1}a_h\Delta l_h+a_{n_{k,i}}\frac{z_{k,i_L}}{\mu_{z_k}}\right)\frac{z}{\mu_{z_k}}\Bigg|_{z_{k,i_L}}^{z_{k,i_U}} \tag{13}$$

2) $\mu_{z_k}=0$, the backtracking direction is perpendicular to the z axis: In this case the bundle travels in the direction normal to the z axis:

$$I_{\text{seg}}(l_k)=\frac{1}{4\pi}\sum_i\sigma_{k,i}\Phi\left(\hat{r},\hat{s}_0,-\hat{s}_k^{\perp}\right)\exp\left(-\sum_j^{m_{k,i}}\kappa_j\Delta z_j-\sum_h^{n_{k,i}-1}a_h\Delta l_h+a_{n_{k,i}}l_{i_L}\right)\int_{l_{k,i}^-}^{l_{k,i}^+}\exp\left(-a_{n_{k,i}}l'\right)\mathrm{d}l' \tag{14}$$

a) $a_{n_{k,i}}\neq 0$:

$$I_{\text{seg}}(l_k)=\frac{1}{4\pi}\sum_i\frac{\sigma_{k,i}\Phi\left(\hat{r},\hat{s}_0,-\hat{s}_k^{\perp}\right)}{a_{n_{k,i}}}\exp\left(-\sum_j^{m_{k,i}}\kappa_j\Delta z_j-\sum_h^{n_{k,i}-1}a_h\Delta l_h+a_{n_{k,i}}l_{i_L}\right)\exp\left(-a_{n_{k,i}}l\right)\Big|_{l_{i_U}}^{l_{i_L}} \tag{15}$$

b) $a_{n_{k,i}}=0$, a purely scattering cell:

$$I_{\text{seg}}(l_{k,i})=\frac{1}{4\pi}\sigma_{k,i}\Phi\left(\hat{r},\hat{s}_0,-\hat{s}_k^{\perp}\right)\times\exp\left(-\sum_j^{m_{k,i}}\kappa_j\Delta z_j-\sum_h^{n_{k,i}-1}a_h\Delta l_h\right)\Delta l \tag{16}$$

where Δl is the traveled distance in that cell perpendicular to the $z$direction.

V. Results and Discussion

The computer system used in the simulation is described in detail in Ref. 5 and will not be repeated here. Figure 4 shows a convenient way to validate the three-dimensional code with the existing, accurate one-dimensional slab solutions obtained with the one-dimensional RMC code and the discrete-ordinates method (DOM).[5,21] The one-dimensional RMC solution was in good agreement with a MC solution developed by another group.[22] The aspect ratio (AR) is the ratio of the width or length over depth of the rectangular participating medium. The depth is in the z-direction (Fig. 2a). The medium has equal width and length in the $z=0$ surface that is subjected to a collimated pulse in the z-axis direction. In this validation case, the whole surface is irradiated with a planar-shaped light pulse to simulate the one-dimensional geometry where a very large AR is used. The standard deviation of three-dimensional RMC results was set to be 1% and that of one-dimensional RMC results was 0.5%. The three-dimensional results show that as the aspect ratio increases from 1 to 100, the transmittance approaches the one-dimensional case. The good agreement of three-dimensional AR = 100 results and one-dimensional results indicate that the three-dimensional RMC code is accurate.

Table 1 Radiative properties of cubic media

Case	τ_1	τ_2	ω_1	ω_2
D11	1	10	0.1	0.9
D14	10	1	0.9	0.1

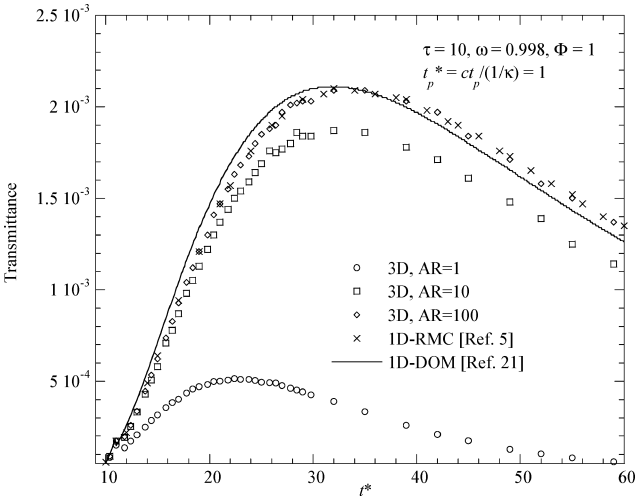

Fig. 4 Validation of three-dimensional RMC code with existing one-dimensional solutions.

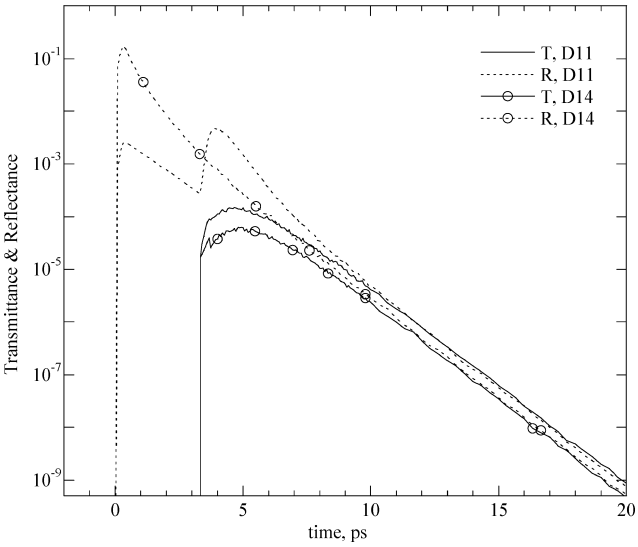

Fig. 5 Reflectance of a three-dimensional cubic medium with two layers in the z direction. Normalized pulse width $t_{po}=0.1$.

Figure 5 and Table 1 show the reflectance (R) and transmittance (T) of the cubic medium with a two-layer structure. T and R are the half-range radiative flux at $x=y=0$ and $z=0$ (R) or $z=1$ mm (T). Two cases D11 and D14 are examined. The interface of the two layers is in the middle, that is, $z=L_0/2=0.5$ mm plane. It is seen that case D11 reflectance has a sudden rise at $t_r=2(L_0/2)/c=3.33$ ps or dual peaks. This is due to the stronger scattering effect in the second layer than in the first layer and the pulse's temporal width at an appropriate scale. The result is consistent with the previous results of the one-dimensional multilayer media.[7] The time of reflectance rise at t_r is exactly the ballistic photons' travel time from the incident surface to the interface and back to the incident surface. Therefore, the temporal reflectance curve has a direct correlation between t_r and the location of the interface, that is, $z=L_0/2$. This is very advantageous in the applications to material property diagnostics or inhomogeneity detection, because the typical inversion procedure will not be needed.

However, such a correlation exists under two conditions, as reported earlier by the authors.[7] These conditions are that 1) the

normalized pulse width ($t_{po} = ct_p/L_0$) has to be less than one and 2) the medium's scattering coefficient before the interface has to be less than that of the medium behind the interface. In the case D14, because the scattering coefficient distribution is exactly opposite to that of case D11, there is no sudden rise in the reflectance curve of D14.

The transmittance curves of Fig. 5 also reveal some interesting phenomena for consideration in the inverse analysis or optical image reconstruction. It has been proposed that the long time logarithm slope (LTLS) of such temporal radiative signal can be used as a parameter for inverse analysis, that is, determination of probed medium's radiative properties. It is clearly seen that both case D11 and D14 have identical LTLS beyond $t = 10$ ps, even though the material property distributions are exactly opposite. This has further confirmed what was reported in our one-dimensional multilayer media study.[7] That is, the LTLS does not provide the specificity needed for an effective inverse analysis.

Additionally, the measurements reported by several groups[23,24] commonly normalized the temporal transmittance signals with their respective peak magnitudes. It has been suggested that the pulse-broadening effect, after normalization, can also be used as an inversion parameter. If one takes Fig. 5, for example, and normalizes the cases D11 and D14 the transmittance curves have their respective peak values at $t = 5$ ps. The two normalized transmittance curves have nearly identical broadened pulse widths. Therefore, this clearly shows that the normalized pulse-broadening effect does not provide the specificity either. The minor difference between the two normalized curves is well below the typical measurement error for such experiment. Figure 5 and previous one-dimensional results clearly indicate that other inversion parameters or temporal information are needed for effective inverse analysis. The new parameters can be used either independently or in conjunction with the broadened pulse width. More work is apparently required to identify any new parameter or temporal information for such use.

Figure 6a is a cubic medium with a highly scattering core in the center. The relevant geometry and radiative property information are given in the figure. Seven detector locations are selected to examine the change of reflectance over time. For the detector locations at $x \leq 5.5$ mm, it is found that the second peak starts at time $t_r = 133.3$ ps, which is again the ballistic photons' travel time from the incident surface to the interface and back (Fig. 6b). Thus, these detectors are able to discern the location of the scattering core region. At detector positions of 8 and 10.5 mm, although there also exists a sudden rise in the reflectance, the rise time is not exactly at t_r. It is larger than t_r. The farther the detector is away from the scattering core, the later is the rise time of the second reflectance peak. This indicates that these two detector positions cannot pick up the signal from ballistic photons. Their signals are coming from the so-called snake photons or slightly scattered photons. Because of the relatively short pulse width in comparison with the depth of the medium (L_0), that is, the normalized pulse width $t_{po} = 0.1$, the appearance of a dual peak or local minimum at t_r is very obvious, as in Fig. 5 case D14.

The results can also be shown in the line-scanned mode (Fig. 6c); that is, the results can be used in direct comparison with the streak camera image, where temporal radiative signal variation along a given detection line path can be obtained. In Fig. 6c, the solid lines are the signal in the first peak group and the dashed lines are the second peak group of Fig. 6b, respectively. Although there are some spatial variations from the 40-ps curve to the 50-ps curve, their general trend is the same: both curves have stronger reflectance signals in the middle. This is an indication of the existence of scattering core. On the other hand, the variations in the second peak group, that is, curves from 130 and 140 to 160 ps, are drastically different. The 130- and 160-ps curves are relatively flat but the 140-ps curve has a sharp drop from the core region ($x = 0$ to 5 mm) toward the outer edge. Of course, a few more detector locations at $x = 6$ to 8 mm will provide higher resolution but the trend of the 140-ps curve is very distinguishable. Such spatial and temporal variations of the reflectance signals closely resemble the measurement in similar configuration[24] and are very useful for inverse analysis. Note

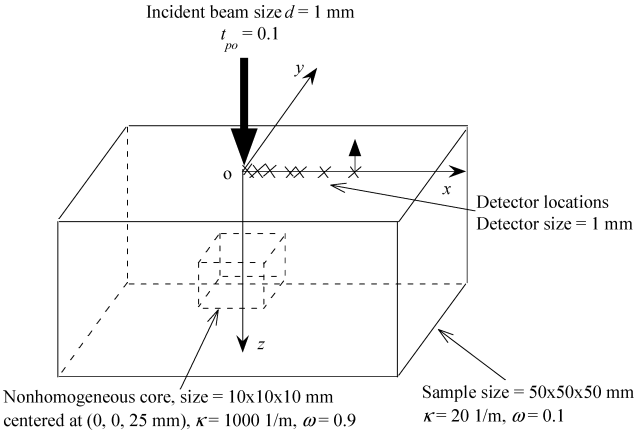

Fig. 6a Detector positions of a three-dimensional cubic medium embedded with a highly scattering core. Detector locations are at $y = z = 0$, $x = 1$, 2, 3, 4.5, 5.5, 8, and 10.5 mm.

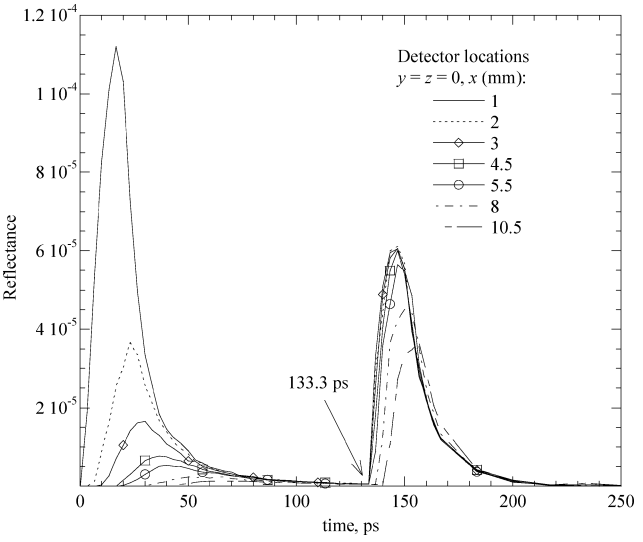

Fig. 6b Reflectances of a three-dimensional cubic medium embedded with a highly scattering core.

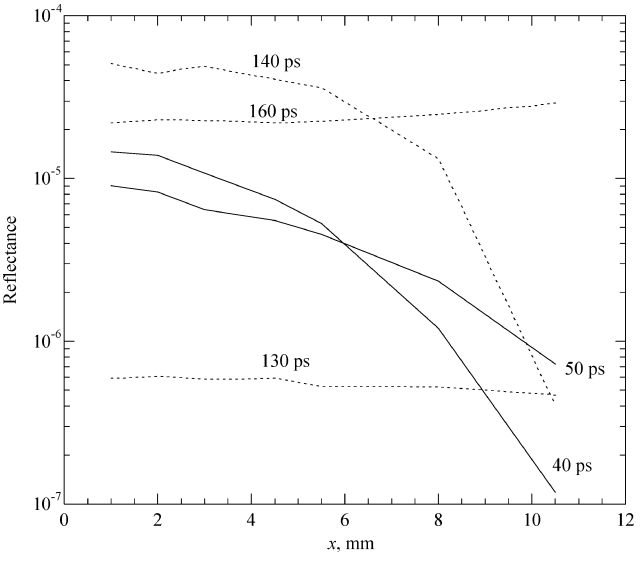

Fig. 6c Line-scanned reflectance temporal history of a three-dimensional cubic medium embedded with a highly scattering core.

that in the experiment reported by Trivedi et al.,[24] a normalized pulse width of $t_{po} = 4.9$ was used (which is far greater than one) and therefore the second peak shown in Fig. 6b would not appear in their measurement. In comparison, the second peak curves (130, 140, and 160 ps) provide more evident and clear indication of the existence of scattering core. This is a clear advantage of using very short pulse width, that is, $t_{po} < 1$. This also suggests that a time-gating detection scheme to capture the second peak signal may be useful for inverse analysis in diagnostic applications.

VI. Conclusions

The reverse Monte Carlo method was developed for a transient radiative transfer process of light-pulse propagation within the absorbing, nonemitting, scattering, and nonhomogeneous three-dimensional media. Detailed treatment of source integration that involves the nonuniform property along the integration path length is given. The reverse Monte Carlo method developed in this study is an accurate and scalable simulation tool to model pulse propagation in the highly scattering media. The temporal reflectance signal from the nonhomogenous medium with scaled pulse width less than one and stronger scattering coefficient in the rear region produces a very unique time–interface location correlation. This is very advantageous in the inverse analysis for optical imaging and remote sensing. Based on the simulated results, it is concluded that the previously proposed inversion parameters, that is, the long-time logarithm slope and pulse-broadening effect, alone are inadequate for use in the inverse analysis because these parameters do not provide the specificity needed for such use. Other parameters are needed, either used independently or in conjunction with the logarithm slope and broadening effect. More work is needed to identify new parameters or temporal information to be used in the inverse analysis.

References

[1]Kumar, S., Hsu, P.-F., Mitra, K., Garetz, B., Guo, Z., and Aber, J., "Radiative Transfer Modeling and Experiments Using Short Pulse Lasers," in *Modeling and Simulation Based Life Cycle Engineering*, Taylor & Francis, New York, 2002.

[2]Lu, X., and Hsu, P.-F., "Parallel Computing of an Integral Formulation of Transient Radiation Transport," *Journal of Thermophysics and Heat Transfer*, Vol. 17, No. 4, 2003, pp. 425–433.

[3]Spanier, J., *Monte Carlo and Quasi-Monte Carlo Methods in Scientific Computing*, edited by H. Niederreiter and P. J. Shiue, Springer-Verlag, New York, 1995, pp. 121–148.

[4]Sawetprawichkul, A., Hsu, P.-F., and Mitra, K., "Parallel Computing of Three-Dimensional Monte Carlo Simulation of Transient Radiative Transfer in Participating Media," AIAA Paper 2002-2901, June 2002.

[5]Lu, X., and Hsu, P.-F., "Reverse Monte Carlo Method for Transient Radiative Transfer in Participating Media," *Proceedings, ASME 2003 International Mechanical Engineering Congress & Exposition*, ASME, New York, Nov. 2003, Paper 2003-41932; also in *Journal of Heat Transfer*, Vol. 126, No. 4, 2004, pp. 621–627.

[6]Lu, X., and Hsu, P.-F., "Reverse Monte Carlo Simulations of Light Pulse Propagation in Nonhomogeneous Media. I. Theoretical Development," *Proceedings, the Fourth International Symposium on Radiation Transfer*, Begell House Inc., New York, 2004.

[7]Lu, X., and Hsu, P.-F., "Reverse Monte Carlo Simulations of Light Pulse Propagation in Nonhomogeneous Media. II: Numerical Simulations," *Proceedings, the Fourth International Symposium on Radiation Transfer*, Begell House Inc., New York, 2004.

[8]Sterling, T., Becker, D. J., Savarese, D., Dorband, J. E., Ranawak, U. A., and Packer, C. V., "Beowulf: A Parallel Workstation for Scientific Computation," *Proceedings of the International Conference on Parallel Processing*, IEEE, Piscataway, NJ, Vol. 1, Aug. 1995, pp. 11–14.

[9]Aber, J., Baretz, B., Guo, Z., and Kumar, S., "Short-Pulse Laser Interactions with Scattering Media: Experimental Results," Mechanical Engineering Dept. Rept., Polytechnic Univ., Brooklyn, NY, June 2001.

[10]Modest, M. F., "Backward Monte Carlo Simulations in Radiative Heat Transfer," *Journal of Heat Transfer*, Vol. 125, No. 1, 2003, pp. 57–62.

[11]Alfano, R. R., Demos, S. G., Galland, P., Gayen, S. K., Cuo, Y., Ho, P. P., Liang, X., Liu, F., Wang, L., Wang, Q. Z., and Wang, W. B., "Time-Resolved and Nonlinear Optical Imaging for Medical Applications," *Annals New York Academy of Science*, Vol. 838, No. 2, 1998, pp. 14–28.

[12]Brusi, A., Sbert, M., Bekaertc, P., Toblerd, R., and Purgathofere, W., "Optimal Ray Shooting in Monte Carlo Radiosity," *Computers and Graphics*, Vol. 26, No. 2, 2002, pp. 351–354.

[13]Nelson, H. F., "Backward Monte Carlo Modeling for Rocket Plume Base Heating," *Journal of Thermophysics and Heat Transfer*, Vol. 6, No. 3, 1992, pp. 556–558.

[14]Walters, D. V., and Buckius, R. O., "Monte Carlo Methods for Radiative Heat Transfer in Scattering Media," *Annual Review of Heat Transfer*, Vol. 5, 1994, pp. 131–176.

[15]Ozisik, M. N., *Radiative Transfer and Interaction with Conduction and Convection*, Wiley, New York, 1973.

[16]Tan, Z.-M., and Hsu, P.-F., "An Integral Formulation of Transient Radiative Transfer," *Journal of Heat Transfer*, Vol. 123, No. 3, 2001, pp. 466–475.

[17]Case, K. M., "Transfer Problems and the Reciprocity Principle," *Review of Modern Physics*, Vol. 29, No. 4, 1957, pp. 651–663.

[18]Olfe, D. B., "Radiative Equilibrium of a Gray Medium Bounded by Nonisothermal Walls," *Progress in Astronautics and Aeronautics*, Vol. 23, 1970, pp. 295–317.

[19]Adams, C. N., and Kattawar, G. W., "Radiative Transfer in Spherical Shell Atmospheres. I. Rayleigh Scattering," *Icarus, International Journal of the Solar Systems*, Vol. 35, 1978, pp. 139–151.

[20]Hsu, P.-F., "Effects of Multiple Scattering and Reflective Boundary on the Transient Radiative Transfer Process," *International Journal of Thermal Science*, Vol. 40, No. 6, 2001, pp. 539–549.

[21]Sakami, M., Mitra, M. K., and Hsu, P.-F., "Transient Radiative Transfer in Anisotropically Scattering Media Using Monotonicity-Preserving Schemes," *ASME 2000 International Mechanical Engineering Congress and Exposition*, Vol. 366-1, ASME, New York, 2000, pp. 135–143.

[22]Wu, C.-Y., "Discrete-Ordinates Solutions and Monte Carlo Simulation for Time-Resolved Radiative Heat Transfer in Two-Layer Media," Rept. NSC-87-2122-E-006-052, National Science Council, Taipei, 1998.

[23]Kumar, S., Guo, Z., Aber, J., and Garetz, B., "Experimental and Numerical Studies of Short Pulse Propagation in Model Systems," *Proceedings, ASME 2002 International Mechanical Engineering Congress and Exposition*, ASME, New York, Paper 2002-33903, 2002.

[24]Trivedi, A., Basu, S., and Mitra, K., "Temporal Analysis of Reflected Optical Signals for Short Pulse Laser Interaction with Nonhomogeneous Tissue Phantoms," *Proceedings, the Fourth International Symposium on Radiation Transfer*, Begell House Inc., New York, 2004.